Applied Catalysis B: Environmental 321 (2023) 122066

Contents lists available at ScienceDirect

Applied Catalysis B: Environmental

journal homepage: www.elsevier.com/locate/apcatb

New insight into the mechanism of symmetry-breaking charge separation induced high-valent iron(IV) for highly efficient photodegradation of organic pollutants

Xin Gao [a], Jianing Li [a], Juan Chen [a], Huinan Che [a], Peifang Wang [a], Bin Liu [b,c], Yanhui Ao [a,*]

[a] Key Laboratory of Integrated Regulation and Resource Development on Shallow Lakes, Ministry of Education, College of Environment, Hohai University, No. 1, Xikang Road, Nanjing 210098, China
[b] School of Chemical and Biomedical Engineering, Nanyang Technological University, Singapore 637459, Singapore
[c] Division of Chemistry and Biological Chemistry, School of Physical and Mathematical Sciences, Nanyang Technological University, 21 Nanyang Link, Singapore 637371, Singapore

ARTICLE INFO

Keywords:
Ligand to metal charge transfer
Photoinduced symmetry-breaking charge separation
Fe(IV)
•OH
Fe^{3+}

ABSTRACT

Fe^{3+} mediating photodegradation of organic pollutants has attracted extensive attention in the field of environment remediation. However, most works focused on low concentration (C_{Fe}<1 mM) system under UV light, in which hydroxyl radicals (•OH) is the main radical for pollutants degradation. In this work, we discover a new mechanism of visible light induced (VLI) symmetry-breaking charge separation for pollutants degradation in high-concentration Fe^{3+} system (HC-Fe^{3+}, C_{Fe}>1 mM). The formed binuclear hydrolyzed Fe^{3+} species ($[(H_2O)_4Fe(\mu\text{-}OH)_2Fe(H_2O)_4]^{4+}$) in HC-$Fe^{3+}$ system significantly broadens the optical absorption range and induces to the generation of Fe(IV), thus leading to highly efficient degradation of organic pollutants. In addition, a logarithmic correlation between the adiabatic ionization potential (AIP) and the reaction rate constant (k) of organics is obtained. The new findings further broaden the knowledge on the generation of Fe(IV) and the photo-induced charge transfer mechanism of binuclear hydrolyzed Fe^{3+} species in the VLIHC-Fe^{3+} system.

1. Introduction

Iron ion (Fe^{3+}) has been widely applied in the mediated oxidation of organic pollutants due to its excellent coordination, valence change ability and spin polarization effect [1–5]. Especially, the catalytic activity of Fe^{3+} is closely related to its existing form. In low-concentration Fe^{3+} solutions (C_{Fe} < 1 mM), the H_2O ligands of $[Fe(H_2O)_6]^{3+}$ is rapidly deprotonated to form mononuclear species with the general formula $[Fe(H_2O)_{6-x}(OH)_x]^{(3-x)+}$ by the polarization of Fe^{3+} with high positive charge density (Eq. (1)) [6–8]. With the increase of Fe^{3+} concentration (C_{Fe} > 1 mM), polynuclear hydrolyzed Fe^{3+} species (e.g., $[(H_2O)_4Fe(\mu\text{-}OH)_2Fe(H_2O)_4]^{4+}$) are formed through the olation process of mononuclear hydrolyzed Fe^{3+} (e.g., $[Fe(H_2O)_5(OH)]^{2+}$) (Eq. (2)) [8–11]. More specifically, the binuclear hydrolyzed Fe^{3+} ($[(H_2O)_4Fe(\mu\text{-}OH)_2Fe(H_2O)_4]^{4+}$) is the simplest and also the only convincingly identified polymeric product [12–15].

$$[Fe(H_2O)_6]^{3+} \rightleftharpoons [Fe(H_2O)_5(OH)]^{2+} \rightleftharpoons [Fe(H_2O)_4(OH)_2]^{+} \quad (1)$$

$$[Fe(H_2O)_5(OH)]^{2+} + [Fe(H_2O)_5(OH)]^{2+} \rightleftharpoons [(H_2O)_4Fe(\mu\text{-}OH)_2Fe(H_2O)_4]^{4+} + 2\ H_2O \quad (2)$$

According to the above-mentioned hydrolysis characteristics of Fe^{3+}, researchers have constructed a Fe^{3+}/UV system based on low-concentration Fe^{3+} (C_{Fe} < 1 mM, mainly in the form of $[Fe(H_2O)_5(OH)]^{2+}$) [16–18]. Compared with Fe^{3+}-H_2O, Fe^{3+}-OH in $[Fe(H_2O)_5(OH)]^{2+}$ has additional electrostatic interactions and forms d-p π-bond between the t_{2g} orbital of Fe^{3+} and the p orbital of OH^-. This leads to the increase of bond energy of Fe^{3+}-OH and the reduction of excitation energy of Fe^{3+} species. Therefore, the low-lying excited states in $[Fe(H_2O)_5(OH)]^{2+}$ are contributed by the ligand-to-metal charge transfer (LMCT) from OH^- to Fe^{3+}, which is responsible for the generation of hydroxyl radicals (•OH) (Eq. (3)). However, previous reports have mainly focused on low-concentration Fe^{3+} systems. In high-concentration Fe^{3+} systems, the photo-induced charge transfer mechanism induced by binuclear hydrolyzed Fe^{3+} species may be

* Corresponding author.
E-mail address: andyao@hhu.edu.cn (Y. Ao).

https://doi.org/10.1016/j.apcatb.2022.122066
Received 6 September 2022; Received in revised form 4 October 2022; Accepted 7 October 2022
Available online 10 October 2022

different from that of mononuclear hydrolyzed Fe^{3+} systems, which has been seriously neglected.

$$[Fe(H_2O)_5(OH)]^{2+} + h\nu \rightarrow [Fe(H_2O)_5]^{2+} + \bullet OH \quad (3)$$

On the other hand, it is well-known that the light absorption range of Fe^{3+} solution can be gradually red-shifted to visible region with the increase of Fe^{3+} concentration (16 mM Fe^{3+} to 510 nm, pH = 2.1) [19]. This is attributed to the formation of binuclear hydrolyzed Fe^{3+} ($[(H_2O)_4Fe(\mu\text{-}OH)_2Fe(H_2O)_4]^{4+}$) in high-concentration solutions [11]. Especially, novel photo-induced charge transfer mechanisms and active species may be generated in $[(H_2O)_4Fe(\mu\text{-}OH)_2Fe(H_2O)_4]^{4+}$ compared with $[Fe(H_2O)_5(OH)]^{2+}$. Similarly, metal to metal charge transfer (MMCT) has been proved to exist in the thermal or optical excitation of polynuclear complexes, involving the d-electron configuration changes and spin cross interactions [20–26]. For instance, Fe(III) and Fe(II) with similar chemical environments in Prussian blue are linked by cyano-bridging ligands, producing a distinct mixed valence spectrum [27]. Simultaneously, for Fe −CN −Co system, when $Fe^{II}_{LS} - CN - Co^{III}_{LS}$ is photoexcited at low temperature, one electron is transferred from the iron (donor) to the cobalt (acceptor) sites to generate the magnetic state $Fe^{III}_{LS} - CN - Co^{II}_{HS}$ [21,22]. Therefore, MMCT can occur in polynuclear mixed-valence metal complexes connected by bridging ligands or conjugated chains. Unfortunately, $[(H_2O)_4Fe(\mu\text{-}OH)_2Fe(H_2O)_4]^{4+}$ contains two high spin Fe^{3+} with opposite spin state and the same valence state, resulting in lacks spontaneous MMCT driving force. Considering the mechanism of non-zero probability of d-d transition in transition metal complexes, the MMCT of $[(H_2O)_4Fe(\mu\text{-}OH)_2Fe(H_2O)_4]^{4+}$ is expected to be initiated by symmetry-breaking. Therefore, the photo-induced symmetry-breaking charge transfer to trigger MMCT and the generation of new active species for $[(H_2O)_4Fe(\mu\text{-}OH)_2Fe(H_2O)_4]^{4+}$ need to be explored deeply.

In recent years, sulfamethoxazole (SMX), a commonly used broad-spectrum and antimicrobial agents, have been identified as a new kind of persistent pollutant and potential threat to the biological environment and human health [28–30]. The study on the degradation characteristics of SMX is conducive to understand the reaction mechanism of sulfonamides at the molecular level and provide the theoretical support for practical applications. Herein, the feature of the absorption edge red-shift with the increase of Fe^{3+} concentration was investigated, which was applied to the efficient degradation of SMX under visible light. In sequence, the mechanism of visible light-induced charge transfer and active species generation was identified in high-concentration Fe^{3+} system. Then, the contribution of photo-induced direct charge transfer between Fe^{3+} and SMX was excluded by the analysis of kinetics, UV–vis absorption spectroscopy and theoretical calculation. Finally, the correlation between the rate constants (k) and adiabatic ionization potential (AIP) of various organic molecules in the VLIHC-Fe^{3+} system was obtained.

2. Methods and materials

2.1. Chemicals and materials

Sources of chemicals and materials are provided in Text S1, Supporting Information.

2.2. Experimental procedure

All experiments were carried out in a 100 mL glass vial containing 50 mL of reaction solution under continuous stirring, with the temperature kept at 25 °C. Generally, batch experiments were performed by adding a predetermined amount of $FeCl_3 \bullet 6\ H_2O$ (abbreviated as Fe^{3+}) and substrates into the vial under magnetic stirring for 5 min to form a homogeneous solution. The initial pH was adjusted to 2.5 by HCl or NaOH and the fluctuation of pH value was less than 0.5 throughout the reaction process. Then, the reaction solution was placed below the preheated Xenon lamp (light intensity: 400 mW cm^{-2}, CEL-HXF300, Beijing China Education Au-light Co., Ltd) equipped with a 400 nm cut-off filter to initiate the photocatalytic reaction. At specific time intervals, 2 mL of the sample was collected and filtered by 0.22 μm PTFE membrane before further analysis. In quenching experiments, a certain amount of IPA and EDTA-2Na were added as the trapping agents of •OH and the complexing agent of Fe^{3+} after the solution contained Fe^{3+} and SMX. In addition, various concentration of DMSO were introduced to demonstrate the effects of Fe(IV) and free radicals, while high purity argon (Ar) was applied to eliminate the interference of O_2. The specific experimental details were the same as described above. All experiments were conducted in duplicate to assure the accuracy and reliability of the data.

2.3. Analytical methods

The concentration of the organic target molecular was analyzed on a high-performance liquid chromatograph (HPLC, Waters e2695, Waters, United States) equipped with a UV–vis detector. The detector conditions including flow rate, wavelength, and ratio of mobile phase were shown in Table S1 (Supporting Information). The ultraviolet-visible (UV–vis) absorption spectra of Fe^{3+} with different molar concentrations were obtained by UV–vis spectrophotometer (UV3600, Shimadzu, Japan). •OH was determined by fluorescence spectrum of 2-hydroxyterephthalic acid derived from the reaction of •OH and TA, and electron spin resonance (ESR, JES-FA200, JEOL, United States) with details displayed in Text S2 and S3, Supporting Information. The concentration measurement of Fe^{2+} and total Fe was also performed on UV3600, whose details were described in Text S4 in the Supporting Information. The degradation intermediates of SMX were determined by ultra-performance liquid chromatography-quadrupole time of flight-mass spectrometer (UPLC-QTOF-MS, Agilent 1290–6550, Agilent, United States), and chromatographic conditions are displayed in the Supporting Information (Text S5).

2.4. Density functional theory (DFT) calculation analysis

The theoretical calculations of isolated systems were performed by Gaussian 16 C.01 [31]. The wave function analysis (e.g., hole-electron analysis [32], interfragment charge transfer (IFCT), UV–vis spectrum and condensed Fukui functions [33–35]) were calculated through Multiwfn 3.8_dev [36]. Details on DFT calculation can be found in Text S6 of the Supplementary data.

3. Results and discussion

3.1. Visible light-induced SMX degradation in the VLIHC-Fe^{3+} system

As is shown in Fig. 1, the photolysis of SMX can be neglected under visible light due to its lack of visible light absorption capability (Fig. S1). Meanwhile, SMX can not directly oxidized by Fe^{3+} under dark. In contrast, VLIHC-Fe^{3+} system exhibit a good photocatalytic activity with 96.0% SMX degradation within 15 min under visible light. Therefore, it is necessary to deeply explore the mechanism on SMX degradation in the VLIHC-Fe^{3+} system.

3.2. Dominant active species produced in the VLIHC-Fe^{3+} system

As shown in Fig. 2a, there are little changes of the photodegradation performance of SMX when oxygen molecules are eliminated through Ar bubbling, indicating that the active species produced in the VLIHC-Fe^{3+} system are not derived from oxygen activation. Besides, the SMX degradation was significantly inhibited with the addition of EDTA, suggesting that the structure of the first coordination sphere of Fe^{3+} significantly affects its photocatalytic activity. Similarly, significant

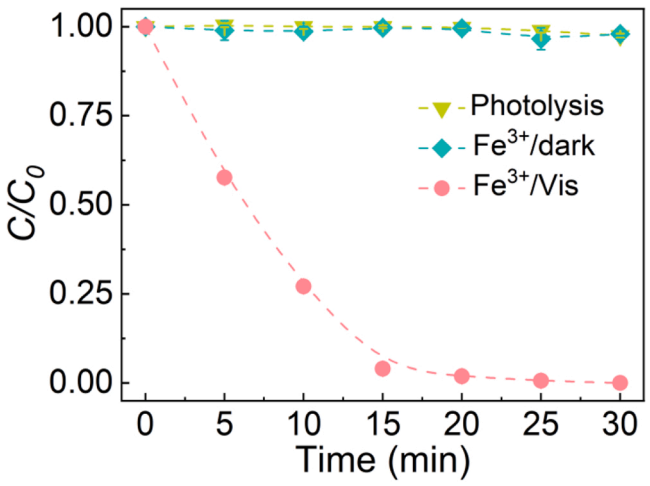

Fig. 1. Degradation of SMX by VLIHC-Fe^{3+} system under visible light irradiation. Experiment condition: [Fe^{3+}] = 5 mM, [SMX] = 20 μM, initial pH = 2.5, and λ ≥ 400 nm.

inhibitory can be observed when *iso*-propanol (IPA) is added to the system. Due to the poor coordination of alcohols, the inhibition of IPA for SMX degradation could be attributed to the quenching of •OH ($k_{•OH,IPA}$ = 1.9 × 10^9 $M^{-1}s^{-1}$) in the VLIHC-Fe^{3+} system [37,38]. Furthermore, ESR technology using DMPO as spin capture agent was further used to verify the generation of •OH in the VLIHC-Fe^{3+} system. As indicated in Fig. 2b, there is no obvious ESR signal under dark conditions. Notably, four DMPO-•OH signals with the relative intensity of 1:2:2:1 is generated, and the intensity of DMPO-•OH signal gradually increase with the extension of illumination time [39]. Meanwhile, the experimental results of qualitative detection of •OH by terephthalic acid (Fig. S2) also exhibit that the fluorescence intensity of •OH is gradually enhanced with the increase of light irradiation time, conforming that •OH can be effectively produced in the VLIHC-Fe^{3+} system [40].

In addition, the high-valent iron(IV) species (Fe(IV)) in the VLIHC-Fe^{3+} system is further surveyed by using DMSO as quenching agent ($k_{Fe(IV),DMSO}$ = 1.26 × 10^5 $M^{-1}s^{-1}$) [41]. The addition of DMSO at a concentration of 10 or 100 mM reduce significantly the degradation rate of SMX to 35% and 27%, respectively (Fig. 2c). However, DMSO also has a strong quenching effect on •OH ($k_{•OH,DMSO}$ = 4.5 × 10^9 $M^{-1}s^{-1}$), thus the above results could not determine the existence of Fe(IV) in the VLIHC-Fe^{3+} system [42]. Fortunately, PMSO can be selectively converted to $PMSO_2$ by Fe(IV) ($k_{Fe(IV),PMSO}$ = 1.23 × 10^5 $M^{-1}s^{-1}$), whereas PMSO oxidation by •OH only yields hydroxylated products (Fig. S3) [41,43–46]. From Fig. 2d, the concentration of PMSO decrease gradually and $PMSO_2$ is eventually produced with the extension of light irradiation time, proving that Fe(IV) species can be generated in the VLIHC-Fe^{3+} system. Simultaneously, the consumption of PMSO&$PMSO_2$ is attributed to the existence of •OH in the VLIHC-Fe^{3+} system ($k_{•OH,PMSO}$ = 3.61 × 10^9 $M^{-1}s^{-1}$ and $k_{•OH,\ PMSO_2}$ = 3.08 × 10^9 $M^{-1}s^{-1}$), which is shown in Fig. 2d and Fig. S4 [44]. Therefore, the results suggest that both •OH and Fe(IV) are the dominant oxidants in the VLIHC-Fe^{3+} system.

3.3. Mechanism of optical absorption and active species production in the VLIHC-Fe^{3+} system

As is shown in Fig. S5, at the same pH value (pH = 2.5), optical absorption edge of Fe^{3+} solution is gradually red-shifted to visible light

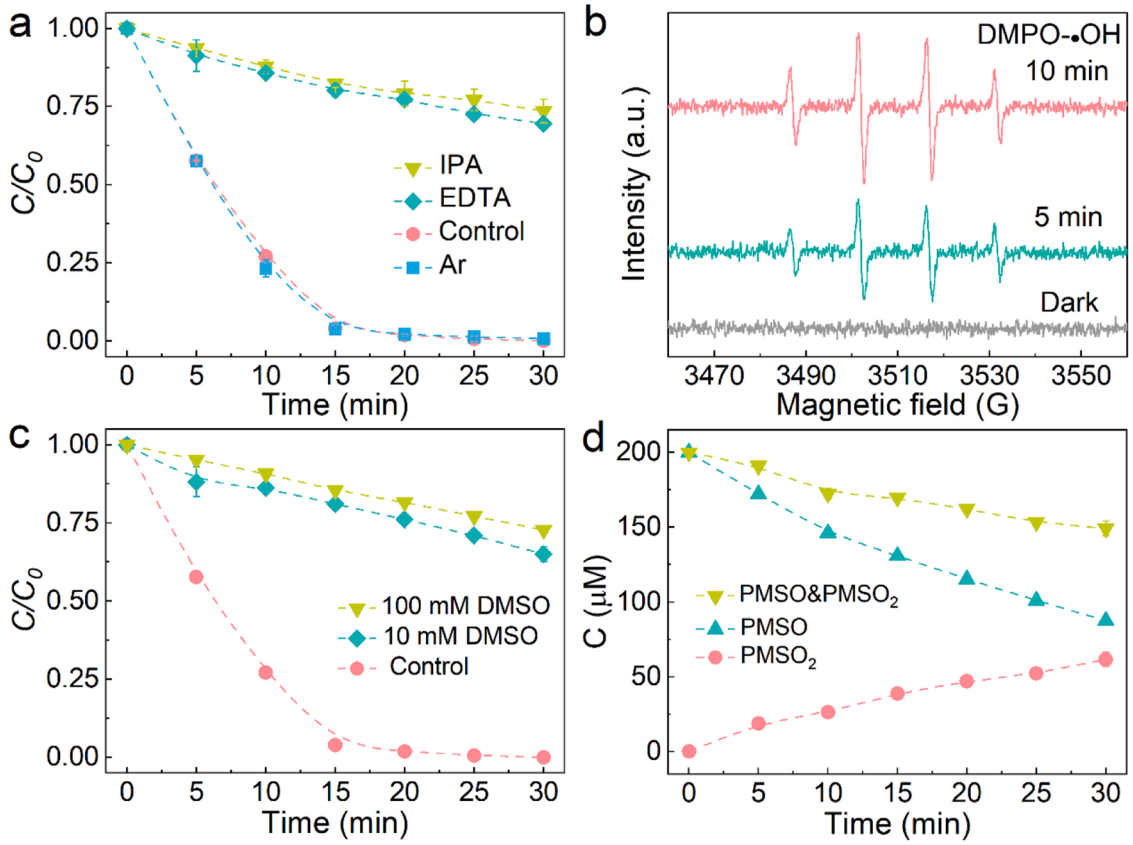

Fig. 2. (a) Degradation effect of SMX by the VLIHC-Fe^{3+} system in the presence of different trapping agents ((a) IPA, EDTA and Ar; (c) DMSO at different concentration). (b) ESR spectrum (DMPO-•OH) and (d) Selective oxidation of PMSO in the VLIHC-Fe^{3+} system. Experiment condition: [Fe^{3+}] = 5 mM, [SMX] = 20 μM, [IPA] = [EDTA] = 10 mM, [DMSO] = 10–100 mM, [DMPO] = 100 mM, [PMSO] = 200 μM, pH = 2.5, and λ ≥ 400 nm.

region with the increase of Fe^{3+} concentration. In particular, when the Fe^{3+} concentration is less than 1.0 mM, the absorption peak is mainly located at about 300 nm. However, when the Fe^{3+} concentration is greater than 1 mM, the absorption peak at about 300 nm disappears and a band-like absorption is formed. Since the solubility product constant ($K_{sp} = 2.8 \times 10^{-39}$) of $Fe(OH)_3$ and pH value remain unchanged, the hydrolysis of Fe^{3+} is correspondingly promoted with increase of Fe^{3+} concentration. In addition, the Fe^{3+} species distribution as a function of concentration and pH is further explored. As shown in Fig. S6, at low concentrations ($C_{Fe} < 1$ mM), Fe^{3+} mainly exists as mononuclear species ($[Fe(H_2O)_6]^{3+}$, $[Fe(H_2O)_5(OH)]^{2+}$, $[Fe(H_2O)_4(OH)_2]^{+}$), while their species distribution remain unchanged with concentration. Interestingly, as the Fe^{3+} concentration increased ($C_{Fe} > 1$ mM), binuclear Fe^{3+} specie ($[(H_2O)_4Fe(\mu\text{-}OH)_2Fe(H_2O)_4]^{4+}$) is formed and their proportion gradually increased. Combined with the characteristics of UV–vis absorption spectra and species distribution, it is speculated that the change of UV–vis absorption spectra and the red-shift of optical absorption edge originate from the formation of $[(H_2O)_4Fe(\mu\text{-}OH)_2Fe(H_2O)_4]^{4+}$ in HC-Fe^{3+} solution [11]. Especially, the degradation performance of SMX gradually improved with the increase of Fe^{3+} concentration (Fig. 3a), indicating that the hydrolyzed Fe^{3+} produced by the increase of Fe^{3+} concentration significantly promote the light absorption and the generation of active species. In addition, the dependence of the high-concentration Fe^{3+} system (5 mM) on the light irradiation range is further discussed. As shown in Fig. 3b, the degradation performance of SMX is rapidly enhanced with the blue-shift of the cutoff wavelength. It is worth noting that when the light absorption range of the high-concentration Fe^{3+} system is completely shielded ($\lambda > 510$ nm), the degradation reaction of SMX is terminated, revealing that the production of active species is closely related to the photoexcitation process of hydrolyzed Fe^{3+}. In conclusion, the moderate hydrolysis of Fe^{3+} are responsible for light absorption and synergistically generating active species.

Furthermore, simulating UV–vis absorption spectra of various forms of Fe^{3+} are employed by theoretical calculations. Obviously, the optical absorption range of $[Fe(H_2O)_6]^{3+}$ is completely in the UV region (Fig. S7), and the absorption peak at 310 nm originates from the LMCT from the H_2O to the Fe^{3+}. In contrast, the optical absorption range of hydrolyzed Fe^{3+} ($[Fe(H_2O)_5(OH)]^{2+}$ and $[(H_2O)_4Fe(\mu\text{-}OH)_2Fe(H_2O)_4]^{4+}$) are significantly expanded to visible light region (Fig. S7). Wherein, $[Fe(H_2O)_5(OH)]^{2+}$ only produces a small absorption peak at 440 nm, while the absorption characteristics of $[(H_2O)_4Fe(\mu\text{-}OH)_2Fe(H_2O)_4]^{4+}$ transform into a band-like structure. Specially, the low-lying excited states of $[Fe(H_2O)_5(OH)]^{2+}$ is mainly composed of LMCT from OH^- to Fe^{3+} (Fig. 4a), indicating that the hydrolysis effect in the HC-Fe^{3+} system introduces a low-energy light absorption unit. Simultaneously, the ligand oxidation (OH^-) and metal ion center (Fe^{3+}) reduction induced by LMCT (IFCT: 0.62 e for S0→S1) will synergistically generate •OH and Fe^{2+}. However, according to the results of species distribution of Fe^{3+}, $[Fe(H_2O)_5(OH)]^{2+}$ exist at various concentrations, implying that the change of spectral characteristics and the red-shift of light absorption range are independent of $[Fe(H_2O)_5(OH)]^{2+}$. Furthermore, the mechanism of visible light induced Fe(IV) production is further explored.

Since high-valence state iron ions (Fe^{3+}) and ligands without electron acceptor ability, it is difficult to enhance the oxidation state of Fe^{3+} in $[Fe(H_2O)_6]^{3+}$, $[Fe(H_2O)_5(OH)]^{2+}$ and $[(H_2O)_4Fe(\mu\text{-}OH)_2Fe(H_2O)_4]^{4+}$ by metal to ligand charge transfer (MLCT). Therefore, considering the transition rule and charge transfer property, the Fe(IV) may be generated by the photoexcitation process of antiferromagnetic $[(H_2O)_4Fe(\mu\text{-}OH)_2Fe(H_2O)_4]^{4+}$. Based on previous studies, Prussian blue, as the most common mixed-valence compound, can produce a distinct mixed-valence spectrum, which originates from the MMCT that occurs between the d orbitals of Fe^{2+} and Fe^{3+} [47,48]. For mixed metal compounds with Prussian-like structure, bidirectional MMCT can also occur under the excitation of light/heat [21,22,24]. Unambiguously, the above-mentioned systems with MMCT are all composed of redox metal ion pairs. Unfortunately, $[(H_2O)_4Fe(\mu\text{-}OH)_2Fe(H_2O)_4]^{4+}$ contains two high spin Fe^{3+} with opposite spin state and the same valence state, resulting in lacks spontaneous MMCT driving force. Meanwhile, since the weak polarization effect of Fe^{2+} on H_2O, $[Fe(H_2O)_6]^{2+}$ is difficult to form mixed valence compounds with $[Fe(H_2O)_6]^{3+}$. Fortunately, Lomoth et al. found out the photo-induced symmetry-breaking charge separation of a transition metal complex ($[Fe^{III}L_2](PF_6)$ (L = [phenyl(tris (3-methylimidazol-1-ylidene))borate]$^-$)) results in the formation of charge separated products ($[Fe^{II}L_2]$ and $[Fe^{IV}L_2]^{2+}$) [49]. Therefore, antiferromagnetic $[(H_2O)_4Fe(\mu\text{-}OH)_2Fe(H_2O)_4]^{4+}$ is considered to possess the possibility of photo-induced symmetry breaking to trigger MMCT. As shown in the Fig. 4b, the d-electron spin states of the two Fe^{3+} ($Fe^{3+}(1)$, left; $Fe^{3+}(2)$, right) in the antiferromagnetic $[(H_2O)_4Fe(\mu\text{-}OH)_2Fe(H_2O)_4]^{4+}$ are opposite, presenting a breaking spin-polarized singlet state. In addition, a schematic diagram of the MMCT mechanism of the antiferromagnetic $[(H_2O)_4Fe(\mu\text{-}OH)_2Fe(H_2O)_4]^{4+}$ based on photo-induced transitions of α-electrons is shown in the middle of Fig. 4b. The d-orbitals of the two Fe^{3+} present the form of mutual donor-acceptor orbitals, which provides the possibility for MMCT. As can be seen from the bottom of Fig. 4b, the frontier molecular orbitals of $[(H_2O)_4Fe(\mu\text{-}OH)_2Fe(H_2O)_4]^{4+}$ are mainly composed of d-orbitals of Fe^{3+}. Wherein, the biorthogonal α-HOMO (singly occupied molecular orbital, SOMO) is e_g*, and the α-LUMO orbital is t_{2g}, indicating that electron in the SOMO can be driven to transition from the e_g* orbit of $Fe^{3+}(1)$ to the virtual orbit of $Fe^{3+}(2)$ under photoexcitation. It can be predicted that the acceptor $Fe^{3+}(2)$ is reduced to Fe^{2+} and Fe(IV) is formed at $Fe^{3+}(1)$. Further, the formation of Fe^{2+} in the VLIHC-Fe^{3+}

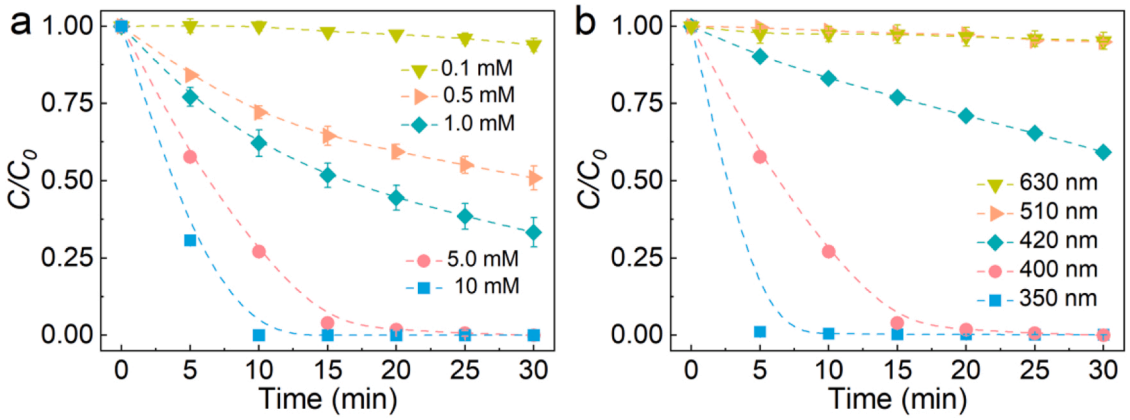

Fig. 3. Effect of (a) Fe^{3+} concentration and (b) light irradiation range on the degradation of SMX. Experiment condition: $[Fe^{3+}] = 0.1$–10 mM, [SMX] = 20 μM, pH = 2.5, and $\lambda \geq 400$ nm.

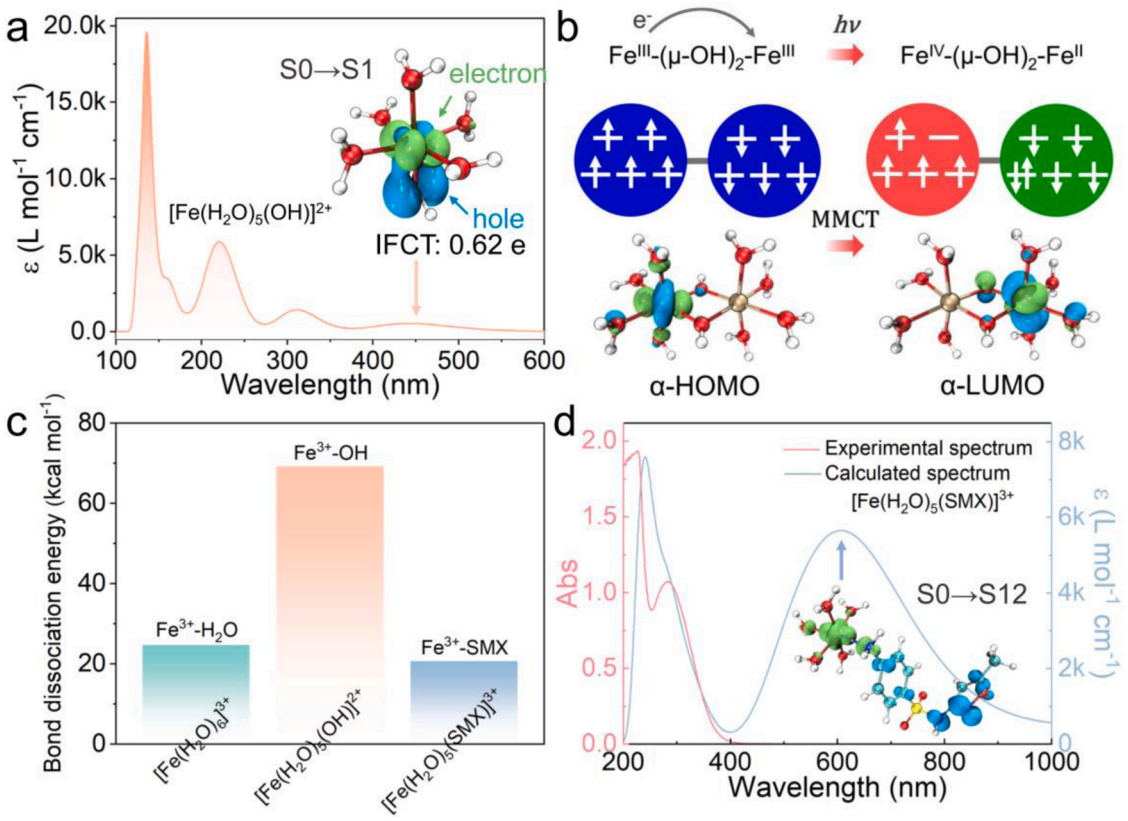

Fig. 4. (a) Simulating UV–vis absorption spectrum and electron-hole analysis of the first excited state of $[Fe(H_2O)_5(OH)]^{2+}$ based on TDDFT; (b) schematic illustration of photo-induced MMCT of $[(H_2O)_4Fe(\mu\text{-}OH)_2Fe(H_2O)_4]^{4+}$; (c) bond dissociation energy of Fe-H_2O, Fe-OH, and Fe-SMX coordinate bond in $[Fe(H_2O)_6]^{3+}$, $[Fe(H_2O)_5(OH)]^{2+}$ and $[Fe(H_2O)_5(SMX)]^{3+}$ based on DFT, respectively; (d) UV–vis absorption spectrum and electron-hole analysis of $[Fe(H_2O)_5(SMX)]^{3+}$.

system is further analyzed. As shown in Fig. S8, no Fe^{2+} is generated under dark. However, when the HC-Fe^{3+} system is exposed under visible light, the proportion of Fe^{2+} gradually increase with the extension of light irradiation time. Moreover, the depletion of active species by SMX further promote the generation and accumulation of Fe^{2+}, proving the existence of photo-induced LMCT and symmetry breaking mechanisms in the VLIHC-Fe^{3+} system. Therefore, the generation of •OH and Fe(IV) originates from the photo-induced LMCT of $[Fe(H_2O)_5(OH)]^{2+}$ and the symmetry-breaking charge separation of antiferromagnetic $[(H_2O)_4Fe(\mu\text{-}OH)_2Fe(H_2O)_4]^{4+}$ in the VLIHC-Fe^{3+} system, respectively.

According to previous reports, there is the contribution of the LMCT mechanism of Fe^{3+}-organic complexes in the UV light-induced low-concentration Fe^{3+} (ULILC-Fe^{3+}) system [50–52]. Thus, the coordination interaction between Fe^{3+} and SMX is further investigated. Initially, the bond dissociation energies (BDE) of Fe^{3+}-H_2O, Fe^{3+}-OH and Fe^{3+}-SMX in $[Fe(H_2O)_6]^{3+}$, $[Fe(H_2O)_5(OH)]^{2+}$, $[Fe(H_2O)_5(SMX)]^{3+}$ complexes are obtained in Table S4, respectively. As shown in Fig. 4c, the BDE of Fe^{3+}-OH is the most negative, conforming that the OH^- in the $[Fe(H_2O)_5(OH)]^{2+}$ is difficult to be replaced by SMX. Compared with that of Fe^{3+}-H_2O, the BDE of Fe^{3+}-SMX is more positive, indicating that coordination water exchange reaction of $[Fe(H_2O)_6]^{3+}$ by SMX is unfavorable. Meanwhile, the Gibbs free energy change of water exchange reaction of $[Fe(H_2O)_6]^{3+}$ by SMX is + 0.42 eV, indicating that the formation of $[Fe(H_2O)_5(SMX)]^{3+}$ is thermodynamically non-spontaneous. In contrast, in the Fe^{3+}-perfluorooctanoic acid (PFOA) system with LMCT mechanism previously reported, PFOA and Fe^{3+} possess more negative BDE (−41.08 kcal mol^{-1}) and Gibbs free energy change (−0.46 eV) of water exchange reaction (Table S4) [52–54]. In addition, simulating UV–vis absorption spectra of $[Fe(H_2O)_5(SMX)]^{3+}$ has a wide visible light response range (Fig. 4d), which is contrary to the experimental spectrum of the mixed solution of Fe^{3+} and SMX (Fig. S9). Namely, there is no coordination interaction between Fe^{3+} and SMX. Meanwhile, the visible light-induced low-concentration Fe^{3+} system (0.1 mM Fe^{3+}) also presents a negligible SMX degradation performance (Fig. 3a). In conclusion, the formation of $[Fe(H_2O)_5(SMX)]^{3+}$ and direct electron transfer between Fe^{3+} and SMX are absent in the Fe^{3+} photocatalytic system, revealing that the degradation of SMX is only contributed by •OH and Fe(IV).

3.4. Structural dependencies of organic molecules degradation in the VLIHC-Fe^{3+} system

To further investigate the effect of structure characteristics for organic molecules degradation in the VLIHC-Fe^{3+} system, the degradation kinetics of various organic molecules were investigated. As shown in Fig. 5a, the excellent degradation performance for phenol, aniline and anisole are observed in the VLIHC-Fe^{3+} system. In contrast, the degradation of benzoic acid, nitrobenzene and benzenesulfonic acid are difficult. Specially, anisole without coordination activity still presents excellent degradation performance, proving that the degradation of organic compounds is not depended on the coordination of Fe^{3+}. In addition, hydroxyl, amino, and methoxy belong to electron-donating groups to activate the benzene, while benzene will be passivated by electron-withdrawing groups (e.g., nitro, carboxyl, and sulfonic acid groups). In particular, •OH and Fe(IV) are respectively non-selective and selective active species, which are more conducive to the oxidation of electron-donor substitution compounds. Interestingly, acetylation reduces the electron donating property of the lone electron pair of the amine group, resulting in a significant decrease in the degradation rate of acetanilide compared with aniline (Fig. 5b). When the electron-donating phenolic hydroxyl group is further introduced into the para position of the acetamido group (acetaminophen), its performance

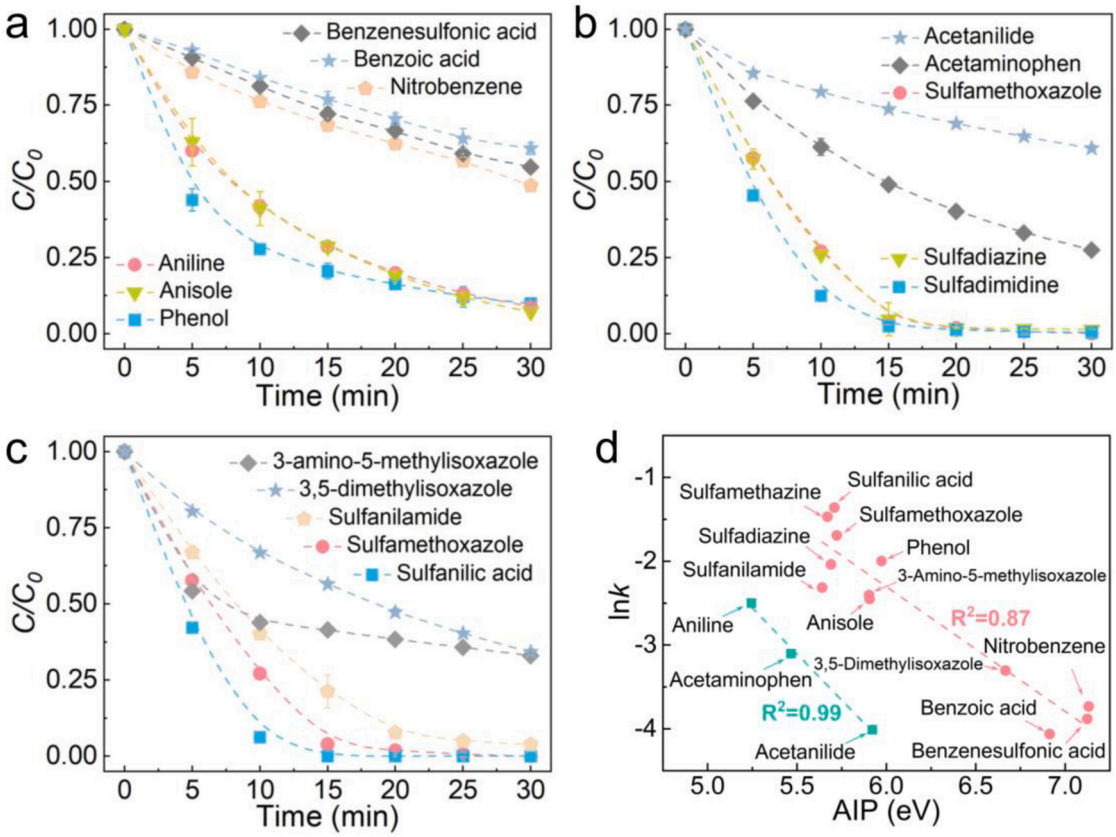

Fig. 5. Degradation performance for (a) monosubstituted benzenes, (b) sulfonamides and aniline organics and (c) SMX fragment in the VLIHC-Fe^{3+} system. (d) relationship between the ln*k* and AIP value. Experimental condition: [Fe^{3+}] = 5 mM, [organic] = 20 μM, pH = 2.5, and λ ≥ 400 nm.

presents a certain recovery. In addition, sulfadiazine and sulfamethazine possess similar degradation performance to SMX. To sum up, the degradation rate of organic compounds is significantly related to their structural characteristics.

In addition, the degradation performance of various fragments of SMX were investigated. According to the structural characteristics of SMX, it can be divided into three fragments, including sulfanilic acid, sulfanilamide, and 3-amino-5-methylisoxazole. Meanwhile, the role of the amine group on isoxazole is investigated through its methyl substitution (3,5-dimethylisoxazole). As shown in Fig. 5c, the sulfanilic acid and sulfanilamide show higher photocatalytic degradation rates compared to the isoxazole ring. Meanwhile, the degradation rate of isoxazole ring is further decreased after the amine group of 3-amino-5-methylisoxazole is substituted by methyl group (3,5-dimethylisoxazole). Therefore, the high degradation performance of the VLIHC-Fe^{3+} system for sulfonamide organics originates from the amino group.

Based on the above analysis, the degradation performance of organic compounds is closely related to their molecular structure. Generally, the degradation of organic molecular originates from active species attack. In particular, the higher the electron cloud density of aromatic ring is, the more favorable it is for the active species to undergo electrophilic attack. Among them, the electron-donating substituent can increase the electron cloud density of the aromatic ring, while electron-withdrawing substituents are the opposite. Furthermore, adiabatic ionization potential (AIP) was introduced to quantify the relationship between the structure and rate constant (*k*) of organics. As shown in the Fig. 5d, ln*k* and AIP have a linear correlation (R^2 =0.87), indicating that the reaction rate decreases exponentially with the increase of the AIP of organic molecules. In addition, aniline organics deviate significantly from the main part, but still show a good linear correlation (R^2 =0.99). This is due to the fact that amine group can be protonated under the condition of pH= 2.5, which will lead to its existence in the form of cation to increase AIP. However, different from common linear correlation between *k* and ionization potential, the exponential decay of *k* with AIP may originate from the simultaneous presence of •OH and Fe(IV) in the VLIHC-Fe^{3+} system. According to literature reports, Fe(IV) is a selective active species ($k_{(Fe(IV,organic)} = 10^0 \sim 10^8 \ M^{-1}s^{-1}$), and a linear correlation is exhibited between rate constant and ionization potential of organic compounds [55]. However, when the ionization potential of organic is greater than a critical point, the reactivity of Fe(IV) is negligible (e.g., benzoic acid and nitrobenzene). The rate constants of •OH with various organic molecules are concentrated in the range of 10^8-10^{10} M^{-1} s^{-1}, indicating non-selective characteristics [43,56]. Therefore, the organic molecules with low ionization potential can be oxidized by both Fe(IV) and •OH. With the increase of ionization potential of organic, the contribution of Fe(IV) gradually decreases, and finally •OH becomes the predominant active species.

4. Conclusion

This paper reveals that the red-shift of the optical absorption edge of HC-Fe^{3+} (C_{Fe} > 1 mM) originates from the generation of $[(H_2O)_4Fe(\mu\text{-}OH)_2Fe(H_2O)_4]^{4+}$. Meanwhile, SMX can be effectively degraded in the VLIHC-Fe^{3+} system, and achieve 96.0% degradation rate within 15 min. In particular, according to the results of quenching experiments, ESR and Fe(IV) detection experiments, it is revealed for the first time that in addition to •OH, Fe(IV) is also detected in the VLIHC-Fe^{3+} system. Wherein, •OH originate from the photo-induced LMCT from OH^- to Fe^{3+} in the $[Fe(H_2O)_5(OH)]^{2+}$, while Fe(IV) produce from the photo-induced symmetry-breaking charge separation of $[(H_2O)_4Fe(\mu\text{-}OH)_2Fe(H_2O)_4]^{4+}$ initiated MMCT between two Fe^{3+}. In addition, based on the results of BDE, Gibbs free energy change and theoretical spectrum of the Fe^{3+}-SMX complex, the formation of $[Fe(H_2O)_5(SMX)]^{3+}$ is thermodynamically non-spontaneous, and the degradation of organic compounds

is not depended on the coordination of Fe^{3+}. Finally, a logarithm correlation between the *k* and AIP for various organics is fitted, indicating the structural dependencies of organic molecules degradation in the VLIHC-Fe^{3+} system. This paper provides new insights into understanding structural-dependent photoinduced charge transfer mechanism and active species production in the Fe^{3+} photocatalytic system.

CRediT authorship contribution statement

Xin Gao: Methodology, Software, Validation, Visualization, Calculation, Writing – original draft. **Jianing Li:** Methodology, Software, Validation, Visualization. **Juan Chen:** Validation, Formal analysis, Writing – review & editing. **Huinan Che:** Validation, Writing – review & editing. **Peifang Wang:** Writing – review & editing, Formal analysis. **Bin Liu:** Formal analysis, Writing – review & editing. **Yanhui Ao:** Conceptualization, Writing – review & editing, Supervision, Funding acquisition, Validation, Formal analysis.

Declaration of Competing Interest

The authors declare that they have no known competing financial interests or personal relationships that could have appeared to influence the work reported in this paper.

Data availability

Data will be made available on request.

Acknowledgments

We are grateful for grants from Natural Science Foundation of China (51979081, 52100179), Fundamental Research Funds for the Central Universities (B200202103), National Science Funds for Creative Research Groups of China (No. 51421006), PAPD, and Postgraduate Research & Practice Innovation Program of Jiangsu Province (KYCX22_0680).

Appendix A. Supplementary material

Supplementary data associated with this article can be found in the online version at doi:10.1016/j.apcatb.2022.122066.

References

[1] S. Sun, S. Wang, Y. Ye, B. Pan, Highly efficient removal of phosphonates from water by a combined Fe(III)/UV/co-precipitation process, Water Res. 153 (2019) 21–28.
[2] M. Zhou, L. Lei, An improved UV/Fe^{3+} process by combination with electrocatalysis for p-nitrophenol degradation, Chemosphere 63 (2006) 1032–1040.
[3] S. Giannakis, M.I.P. López, D. Spuhler, J.A.S. Pérez, P.F. Ibáñez, C. Pulgarin, Solar disinfection is an augmentable, in situ-generated photo-Fenton reaction—part 1: a review of the mechanisms and the fundamental aspects of the process, Appl. Catal. B Environ. 199 (2016) 199–223.
[4] S.J. Hug, L. Canonica, M. Wegelin, D. Gechter, U. Von, Gunten, Solar oxidation and removal of arsenic at circumneutral pH in iron containing waters, Environ. Sci. Technol. 35 (2001) 2114–2121.
[5] D.-h Kim, D. Lee, D. Monllor-Satoca, K. Kim, W. Lee, W. Choi, Homogeneous photocatalytic Fe^{3+}/Fe^{2+} redox cycle for simultaneous Cr(VI) reduction and organic pollutant oxidation: roles of hydroxyl radical and degradation intermediates, J. Hazard. Mater. 372 (2019) 121–128.
[6] C. Baes, R. Mesmer. The Hydrolysis of Cations, Jobo Wiley and Sons, New York, 1976.
[7] J.S. Weatherill, K. Morris, P. Bots, T.M. Stawski, A. Janssen, L. Abrahamsen, R. Blackham, S. Shaw, Ferrihydrite formation: the role of Fe_{13} Keggin clusters, Environ. Sci. Technol. 50 (2016) 9333–9342.
[8] M. Zhu, C. Frandsen, A.F. Wallace, B. Legg, S. Khalid, H. Zhang, S. Mørup, J. F. Banfield, G.A. Waychunas, Precipitation pathways for ferrihydrite formation in acidic solutions, Geochim. Cosmochim. Acta 172 (2016) 247–264.
[9] J. Dousma, P. Bruyn, Hydrolysis-precipitation studies of iron solutions. I. Model for hydrolysis and precipitation from Fe(III) nitrate solutions, J. Colloid Interface Sci. 56 (1976) 527–539.
[10] M.A. Blesa, E. Matijević, Phase transformations of iron oxides, oxohydroxides, and hydrous oxides in aqueous media, Adv. Colloid Interface Sci. 29 (1989) 173–221.
[11] M. Zhu, B.W. Puls, C. Frandsen, J.D. Kubicki, H. Zhang, G.A. Waychunas, In situ structural characterization of ferric iron dimers in aqueous solutions: identification of mu-oxo species, Inorg. Chem. 52 (2013) 6788–6797.
[12] H. Schugar, G.R. Rossman, H.B. Gray, Dihydroxo-bridged ferric dimer, J. Am. Chem. Soc. 91 (1969) 4564–4566.
[13] M.K. Coggins, S. Toledo, J.A. Kovacs, Isolation and characterization of a dihydroxo-bridged iron (III, III)(μ-$OH)_2$ diamond core derived from dioxygen, Inorg. Chem. 52 (2013) 13325–13331.
[14] C.M. Flynn, Hydrolysis of inorganic iron(III) salts, Chem. Rev. 84 (1984) 31–41.
[15] R.H. Byrne, Y.R. Luo, R.W. Young, Iron hydrolysis and solubility revisited: observations and comments on iron hydrolysis characterizations, Mar. Chem. 70 (2000) 23–35.
[16] Y. Sun, J.J. Pignatello, Organic intermediates in the degradation of 2, 4-dichlorophenoxyacetic acid by iron (3+)/hydrogen peroxide and iron (3+)/hydrogen peroxide/UV, J. Agric. Food Chem. 41 (1993) 1139–1142.
[17] Y. Sun, J.J. Pignatello, Photochemical reactions involved in the total mineralization of 2, 4-D by iron (3+)/hydrogen peroxide/UV, Environ. Sci. Technol. 27 (1993) 304–310.
[18] J. Ma, W. Ma, W. Song, C. Chen, Y. Tang, J. Zhao, Y. Huang, Y. Xu, L. Zang, Fenton degradation of organic pollutants in the presence of low-molecular-weight organic acids: cooperative effect of quinone and visible light, Environ. Sci. Technol. 40 (2006) 618–624.
[19] Y. Wang, H. Suzuki, J. Xie, O. Tomita, D.J. Martin, M. Higashi, D. Kong, R. Abe, J. Tang, Mimicking natural photosynthesis: solar to renewable H_2 fuel synthesis by Z-scheme water splitting systems, Chem. Rev. 118 (2018) 5201–5241.
[20] A. Bleuzen, V. Marvaud, C. Mathoniere, B. Sieklucka, M. Verdaguer, Photomagnetism in clusters and extended molecule-based magnets, Inorg. Chem. 48 (2009) 3453–3466.
[21] C. Mathonière, Metal-to-metal electron transfer: a powerful tool for the design of switchable coordination compounds, Eur. J. Inorg. Chem. 2017 (2018) 248–258.
[22] D. Aguila, Y. Prado, E.S. Koumousi, C. Mathoniere, R. Clerac, Switchable Fe/Co Prussian blue networks and molecular analogues, Chem. Soc. Rev. 45 (2016) 203–224.
[23] C.Q. Jiao, Y.S. Meng, Y. Yu, W.J. Jiang, W. Wen, H. Oshio, Y. Luo, C.Y. Duan, T. Liu, Effect of intermolecular interactions on metal-to-metal charge transfer: a combined experimental and theoretical investigation, Angew. Chem. Int. Ed. 131 (2019) 17165–17171.
[24] Y.S. Meng, O. Sato, T. Liu, Manipulating metal-to-metal charge transfer for materials with switchable functionality, Angew. Chem. Int. Ed. 57 (2018) 12216–12226.
[25] S.-i Ohkoshi, H. Tokoro, Photomagnetism in cyano-bridged bimetal assemblies, Acc. Chem. Res. 45 (2012) 1749–1758.
[26] M. Lenglet, C.K. Jørgensen, Influence of the antiferromagnetic interaction associated with octahedral Fe^{3+}-Ni^{2+} on the optical spectra in oxides, Chem. Phys. Lett. 197 (1992) 259–264.
[27] F.S. Hegner, J.R. Galan-Mascaros, N. Lopez, A database of the structural and electronic properties of prussian blue, prussian white, and berlin green compounds through density functional theory, Inorg. Chem. 55 (2016) 12851–12862.
[28] M. Al Aukidy, P. Verlicchi, A. Jelic, M. Petrovic, D. Barcelò, Monitoring release of pharmaceutical compounds: occurrence and environmental risk assessment of two WWTP effluents and their receiving bodies in the Po Valley, Italy, Sci. Total Environ. 438 (2012) 15–25.
[29] N. Ratola, A. Cincinelli, A. Alves, A. Katsoyiannis, Occurrence of organic microcontaminants in the wastewater treatment process. A mini review, J. Hazard. Mater. 239–240 (2012) 1–18.
[30] L.P. Padhye, H. Yao, F.T. Kung'u, C.H. Huang, Year-long evaluation on the occurrence and fate of pharmaceuticals, personal care products, and endocrine disrupting chemicals in an urban drinking water treatment plant, Water Res. 51 (2014) 266–276.
[31] M.J. Frisch, G.W. Trucks, H.B. Schlegel, G.E. Scuseria, M.A. Robb, J.R. Cheeseman, G. Scalmani, V. Barone, G.A. Petersson, H. Nakatsuji, X. Li, M. Caricato, A.V. Marenich, J. Bloino, B.G. Janesko, R. Gomperts, B. Mennucci, H.P. Hratchian, J.V. Ortiz, A.F. Izmaylov, J.L. Sonnenberg, Williams, F. Ding, F. Lipparini, F. Egidi, J. Goings, B. Peng, A. Petrone, T. Henderson, D. Ranasinghe, V.G. Zakrzewski, J. Gao, N. Rega, G. Zheng, W. Liang, M. Hada, M. Ehara, K. Toyota, R. Fukuda, J. Hasegawa, M. Ishida, T. Nakajima, Y. Honda, O. Kitao, H. Nakai, T. Vreven, K. Throssell, J.A. Montgomery Jr, J.E. Peralta, F. Ogliaro, M.J. Bearpark, J.J. Heyd, E. N. Brothers, K.N. Kudin, V.N. Staroverov, T.A. Keith, R. Kobayashi, J. Normand, K. Raghavachari, A.P. Rendell, J.C. Burant, S.S. Iyengar, J. Tomasi, M. Cossi, J.M. Millam, M. Klene, C. Adamo, R. Cammi, J.W. Ochterski, R.L. Martin, K. Morokuma, O. Farkas, J.B. Foresman, D.J. Fox, Gaussian 16 Rev. C.01, Wallingford, CT, 2016.
[32] Z. Liu, T. Lu, Q. Chen, An sp-hybridized all-carboatomic ring, cyclo [18] carbon: electronic structure, electronic spectrum, and optical nonlinearity, Carbon 165 (2020) 461–467.
[33] R.G. Parr, W. Yang, Density functional approach to the frontier-electron theory of chemical reactivity, J. Am. Chem. Soc. 106 (1984) 4049–4050.
[34] P.W. Ayers, R.G. Parr, Variational principles for describing chemical reactions: the Fukui function and chemical hardness revisited, J. Am. Chem. Soc. 122 (2000) 2010–2018.
[35] P. Fuentealba, P. Pérez, R. Contreras, On the condensed Fukui function, J. Chem. Phys. 113 (2000) 2544–2551.
[36] T. Lu, F. Chen, Multiwfn: a multifunctional wavefunction analyzer, J. Comput. Chem. 33 (2012) 580–592.

[37] Yn Wang, J. Chen, X. Li, S. Zhang, X. Qiao, Estimation of aqueous-phase reaction rate constants of hydroxyl radical with phenols, alkanes and alcohols, QSAR & Comb. Sci. 28 (2009) 1309–1316.
[38] L. Wang, B. Li, D.D. Dionysiou, B. Chen, J. Yang, J. Li, Overlooked formation of H_2O_2 during the hydroxyl radical-scavenging process when using alcohols as scavengers, Environ. Sci. Technol. 56 (2022) 3386–3396.
[39] X. Gao, J. Chen, H. Che, Y. Ao, P. Wang, Rationally constructing of a novel composite photocatalyst with multi charge transfer channels for highly efficient sulfamethoxazole elimination: mechanism, degradation pathway and DFT calculation, Chem. Eng. J. 426 (2021), 131585.
[40] X. Gao, C. Ma, Y. Liu, L. Xing, Y. Yan, Self-induced Fenton reaction constructed by Fe(III) grafted $BiVO_4$ nanosheets with improved photocatalytic performance and mechanism insight, Appl. Surf. Sci. 467–468 (2019) 673–683.
[41] O. Pestovsky, A. Bakac, Aqueous ferryl (IV) ion: kinetics of oxygen atom transfer to substrates and oxo exchange with solvent water, Inorg. Chem. 45 (2006) 814–820.
[42] H. Bardouki, M.B. Da Rosa, N. Mihalopoulos, W.-U. Palm, C. Zetzsch, Kinetics and mechanism of the oxidation of dimethylsulfoxide (DMSO) and methanesulfinate (MSI−) by OH radicals in aqueous medium, Atmos. Environ. 36 (2002) 4627–4634.
[43] Z. Wang, W. Qiu, S.Y. Pang, Q. Guo, C. Guan, J. Jiang, Aqueous iron(IV)-oxo complex: an emerging powerful reactive oxidant formed by iron(II)-based advanced oxidation processes for oxidative water treatment, Environ. Sci. Technol. 56 (2022) 1492–1509.
[44] Z. Wang, J. Jiang, S. Pang, Y. Zhou, C. Guan, Y. Gao, J. Li, Y. Yang, W. Qiu, C. Jiang, Is sulfate radical really generated from peroxydisulfate activated by iron (II) for environmental decontamination? Environ. Sci. Technol. 52 (2018) 11276–11284.
[45] N. Jiang, H. Xu, L. Wang, J. Jiang, T. Zhang, Nonradical oxidation of pollutants with single-atom-Fe(III)-activated persulfate: Fe(V) being the possible intermediate oxidant, Environ. Sci. Technol. 54 (2020) 14057–14065.
[46] J. Liang, X. Duan, X. Xu, K. Chen, Y. Zhang, L. Zhao, H. Qiu, S. Wang, X. Cao, Persulfate oxidation of sulfamethoxazole by magnetic iron-char composites via nonradical pathways: Fe(IV) versus surface-mediated electron transfer, Environ. Sci. Technol. 55 (2021) 10077–10086.
[47] R. Glauser, U. Hauser, F. Herren, A. Ludi, P. Roder, E. Schmidt, H. Siegenthaler, F. Wenk, Mixed valence spectrum and cyclic voltammetry of binuclear iron cyano complexes, J. Am. Chem. Soc. 95 (1973) 8457–8458.
[48] K.S. Hagen, S.G. Naik, B.H. Huynh, A. Masello, G. Christou, Intensely colored mixed-valence iron(II) iron(III) formate analogue of prussian blue exhibits Néel N-type ferrimagnetism, J. Am. Chem. Soc. 131 (2009) 7516–7517.
[49] N. Kaul, R. Lomoth, The carbene cannibal: photoinduced symmetry-breaking charge separation in an Fe(III) N-heterocyclic carbene, J. Am. Chem. Soc. 143 (2021) 10816–10821.
[50] R. Yin, Y. Chen, J. Hu, G. Lu, L. Zeng, W. Choi, M. Zhu, Complexes of Fe(III)-organic pollutants that directly activate Fenton-like processes under visible light, Appl. Catal. B Environ. 283 (2021), 119663.
[51] Y. Yuan, L. Feng, N. Xie, L. Zhang, J. Gong, Rapid photochemical decomposition of perfluorooctanoic acid mediated by a comprehensive effect of nitrogen dioxide radicals and Fe(3+)/Fe(2+) redox cycle, J. Hazard. Mater. 388 (2020), 121730.
[52] Y. Wang, P. Zhang, G. Pan, H. Chen, Ferric ion mediated photochemical decomposition of perfluorooctanoic acid (PFOA) by 254 nm UV light, J. Hazard. Mater. 160 (2008) 181–186.
[53] L. Jin, P. Zhang, T. Shao, S. Zhao, Ferric ion mediated photodecomposition of aqueous perfluorooctane sulfonate (PFOS) under UV irradiation and its mechanism, J. Hazard. Mater. 271 (2014) 9–15.
[54] J.-h Cheng, X.-y Liang, S.-w Yang, Y.-y Hu, Photochemical defluorination of aqueous perfluorooctanoic acid (PFOA) by VUV/Fe^{3+} system, Chem. Eng. J. 239 (2014) 242–249.
[55] J. Wang, K.P. Hou, Y. Wen, H. Liu, H. Wang, K. Chakarawet, M. Gong, X. Yang, Interlayer structure manipulation of iron oxychloride by potassium cation intercalation to steer H_2O_2 activation pathway, J. Am. Chem. Soc. 144 (10) (2022) 4294–4299.
[56] Z. Yang, J. Qian, C. Shan, H. Li, Y. Yin, B. Pan, Toward selective oxidation of contaminants in aqueous systems, Environ. Sci. Technol. 55 (2021) 14494–14514.